DYNAMIC LOADING ON PUMPS—CAUSES FOR VIBRATIONS

by

Stefan Florjancic

Senior Field Engineer

Sulzer Bingham Pumps Inc., Portland, OR

and

Arno Frei

Head, Mechanical Development Group

Sulzer Brothers Limited

Winterthur, Switzerland

Stefan S. Florjancic graduated (1982) from the Federal Institute of Technology in Zurich, Switzerland, with a degree in Mechanical Engineering. After training periods in pump factories in Switzerland, West Germany, U.S.A., France, and Brazil, he joined Sulzer Brothers, Limited, in Switzerland (1983). He worked seven years in the area of mechanical development and design of pumps, mainly covering rotordynamic calculations and research. He received a Ph.D. degree for a combined experimental and theoretical research theses covering the rotordynamic influence of annular seals from the Federal Institute of Technology, in Zurich (1990).

Dr. Florjancic then joined Sulzer Bingham Pumps, Inc., in Portland, Oregon, where he works as a Senior Field Engineer. His responsibilities include general troubleshooting, vibration data acquisition and analysis of pump installations, and mechanical and rotordynamic advising on pump designs.

Arno Frei graduated (1959) from St. Gall Technical College, Switzerland, with a degree in Mechanical Engineering. He joined Sulzer in 1966 and was first engaged in the design and development of primary recirculation pumps for nuclear power stations. After activities in the field of nuclear heat exchangers, he rejoined the pump division, where he has been Head of the Mechanical Development Group since 1978.

ABSTRACT

Some insight into the mechanisms which generate lateral dynamic loads, and hence vibrations, on centrifugal pumps is presented in a general way, and the individual loads are explained and quantified. Without extensive use of formulas and equations, this information can identify the significant types of forces and separate them from less important ones.

Measured data of lateral dynamic forces and resulting vibrations on pumps are presented, the individual causes are identified, and means to reduce specific loading forces are shown. However, loading forces cannot be eliminated totally. Therefore, approximate levels of forces which have to be accepted as physical properties of a centrifugal pump are established.

The particular comparison of mechanical versus hydraulic loading forces consequently leads to the definition of reasonable limits on mechanical balancing and rotor runout. When mechanical loading forces become much smaller than hydraulic forces, tighter manufacturing tolerances will not further improve the overall vibration behavior.

INTRODUCTION

It is commonly known that vibration problems on a centrifugal pump can result from a multitude of possible parameters which are not easily identified. Yet, in order to find a remedy, the cause of the vibration must be first understood and found. An overview of various root causes for vibrations in multistage pumps is given in APPENDIX A, [1].

Generally, there are two principle areas to be investigated, as outlined in Figure 1. Either the dynamic pump rotor-casing-baseplate system is resonant or close to resonance (e.g., at a critical speed or at a bearing housing resonance), or the forces driving the vibrations are excessive. Hence, depending on the nature of the problem, either the system dynamics need to be changed, or the loading forces need to be identified and reduced.

Descriptions on how to model a pump as a dynamic system in order to calculate its natural frequencies and corresponding damping values can be found in many publications [2], [3], [4]. An

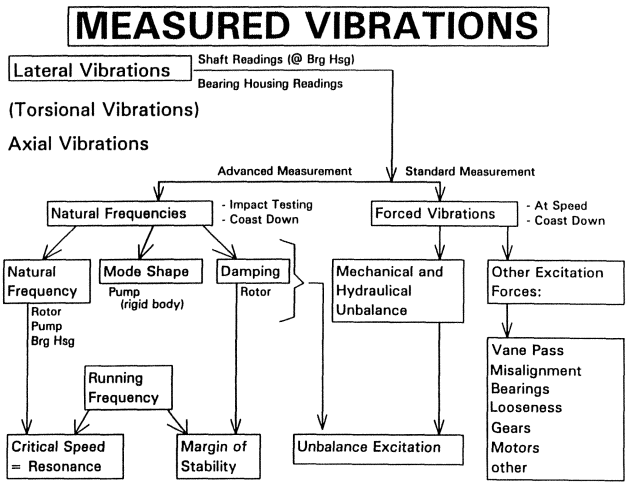

Figure 1. Resonant and Stability Problems Vs *Forced Vibration Problems.*

approach on how to measure system properties is described in [5]. The model of a pump as a dynamic system allows the identification of stability limits, critical speeds, and generally how sensitive the machine is to excitation forces at certain frequencies (i.e., natural frequencies) and at certain locations (i.e., antinodal points). Interpretation of results and means to change the dynamic system are well described in the literature.

The focus of this presentation is on the identification and quantification of dynamic loading forces driving the vibrations in a pump. Unlike the measurement of dynamic pump system properties, the measurement of forced vibrations is much more straight forward, as the loading or excitation forces are always present. They are to be distinguished from interaction forces, e.g., in eye ring and hub ring seals, impeller-casing interaction, etc., which are only present when the pump rotor vibrates. Interaction forces are part of the pump dynamic system model and are not discussed here.

In Figure 2, various areas for potential dynamic loading forces are indicated. They can be caused by hydraulic or mechanical problems and can be summarized as:

Mechanical

- Mechanical unbalance
- Bent shaft
- Component runout

Hydraulic

- Hydraulic unbalance
- Vane passage forces
- Forces due to recirculation/separation, rotating stall and similar phenomena
- Excitation due to cavitation
- Surge and system instabilities

Other mechanical problems, e.g., misalignment, soft foot, etc., are not treated here, as they are not inherent pump problems, but result from an inappropriate machine setup.

Most of the listed excitation forces are best presented in a normalized form, which makes them largely (though not entirely) independent of the machine size and design. In order to get a better feeling for the effective forces acting on the pump, two numerical examples are given for each force. The anticipated levels of the dynamic loading forces are indicated on the example of a four stage, stacked impeller design pump with a barrel casing (A) and a 14 stage back to back design with a horizontally split casing (B), Figures 2 and 3, respectively.

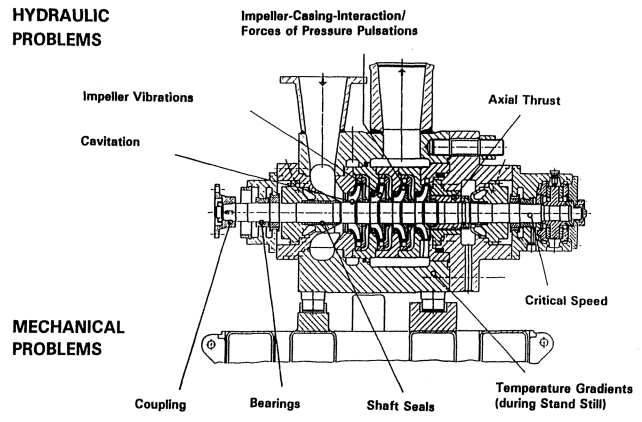

Figure 2. Different Origins of Loading Forces (Cross Section of Pump A).

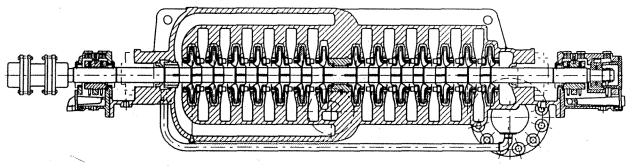

Figure 3. Cross Section of Pump B.

The energy concentration EC of a pump may be defined by the energy per stage divided by the projected impeller area:

$$EC = rho \cdot g \cdot H \cdot Q \cdot 4 / (D_2^2 \cdot Pi) \quad \text{(metric)} \qquad (1)$$

Pump A with EC = 18.8 MW/m² (2340 BHP/ft²) is a high energy concentration pump, while pump B with EC = 1.7 (211 BHP/ft²) is a low energy concentration unit. Therefore, the different types of design also imply totally different specific energy levels for the two pumps. The differences in design and energy levels lead to substantially different levels of dynamic loading forces for the two units.

Table 1. Main Dimensions of the Two Types of Pumps.

	Pump A		Pump B			
Head	2195	(7201)	1829	(6000)	m	(ft)
Head per Stage, H	549	(1800)	131	(429)	m	(ft)
Flow, Q	0.335	(5310)	0.063	(1000)	m^3/s	(GPM)
Speed, N	6200		3560		RMP	
Rotor Mass	444	(979)	190	(419)	kg	(lb)
Number of Stages	4		14		-	
Specific Speed	32	(1635)	23	(1195)	-	
Impeller Mass	16	(35)	5.6	(12.5)	kg	(lb)
Impeller Diameter, D_2	0.333	(13.1)	0.238	(9.4)	m	(in)
Imp. Outlet Width, B_2*	0.038	(1.5)	0.032	(1.3)	m	(in)
Fluid Density, rho	907	(57.9)	945	(59.0)	kg/m^3	(lb/ft^3)

DYNAMIC LOADING FORCES

Mechanical

Mechanical Unbalance

Mechanical unbalance is the most well-known excitation force and most often suspected to be the cause of vibrations in a centrifugal pump. It causes vibrations at exactly running frequency. Though mechanical unbalance is a very likely cause, measurement of synchronous vibration does not necessarily mean that the rotor is badly out of mechanical balance, as there are many other causes which lead to synchronous vibrations (hydraulic unbalance, temporary or permanent rotor bow, casing distortion, critical speed, misalignment, etc.).

On a stiff shaft, unbalance causes a force of

$$F_m = omega^2 \cdot U \qquad (2)$$

where U is the unbalance in [kg·m] or [oz·in]/(16.386.4). There are various balance standards which can be applied. The standard ISO 1940 [6] gives various grades of allowable residual unbalance G, normally used are G=6.3 and G = 2.5. According to ISO 1940, G = 6.3 is to be used for "pump impellers, fans, fly wheels, components under special requirements" among others. The more restrictive G = 2.5 is to be used for "gas and steam turbines,

turbo-compressors, machine tool-drives, turbine driven (= high speed) pumps" and others. The classification suggests that G = 6.3 is to be used for "general" turbomachinery, and G = 2.5 is to be used for more "sophisticated" or sensitive turbomachinery.
The unbalance is calculated to be

$$\begin{aligned} U &= G \cdot Mass \cdot 10^{-3} / omega \quad [kg{\cdot}m] \quad (\text{"Mass" in [kg]}) \\ U &= G \cdot Mass \cdot 0.6299 / omega \quad [oz{\cdot}in] \quad (\text{"Mass" in [lb]}) \end{aligned} \tag{3}$$

API 610, 7th Edition [7], indicates the following rule for residual unbalance:

$$\begin{aligned} U &= 6350 \cdot W / N \cdot 10^{-6} \quad [kg{\cdot}m] \quad (\text{"Mass" in [kg]}) \\ U &= \quad 4 \cdot W / N \quad [oz{\cdot}in] \quad (\text{"Mass" in [lb]}) \end{aligned} \tag{4}$$

Hence, API 610 leads to values almost four times smaller than ISO G = 2.5 ("G ≈ 0.7 in). It is interesting to note that ISO 1940 G = 1 classifies "tape recorder and phonograph drivers, and grinding machine drivers."

In order to calculate the unbalance force on a per stage base, the total rotor mass is divided by the number of stages. The resulting unbalance forces are indicated in Table 2 for the two sample pumps.

Table 2. Residual Unbalance Excitation Forces.

	Force per Stage		Force of Entire Pump		
	Pump A	Pump B	Pump A	Pump B	
ISO G - 6.3	454 (102)	32 (7)	1816 (408)	446 (100)	N (lb.f.)
ISO G = 2.5	180 (40)	13 (3)	721 (162)	177 (40)	N (lb.f.)
API 610	48 (11)	3.4 (0.8)	192 (43)	47 (11)	N (lb.f.)

It can be seen, that the rule by API is substantially more stringent than the lower ISO limit for residual unbalance. Caused by the differences in the rotor mass, the rotor speed, and the number of stages, the allowable unbalance loading forces vary widely. For pump A, the force on the entire pump is 4 × bigger and the force per stage is 14 × bigger than for pump B.

These dynamic forces have to be compared to excitation forces caused by other effects. Additionally, it has to be recognized what average mass eccentricity, e_{unb}, the individual unbalance limits represent. This value can be calculated based on U and the total rotor mass, Equation (5), and the results are presented in Table 3.

$$e_{unb} = U / (Rotor\_mass) \tag{5}$$

Table 3. Average Mass Eccentricity Due to Unbalance Limits.

	Average Mass Eccentricity				
	Pump A		Pump B		
ISO G = 6.3	9.7	(0.38)	16.9	(0.67)	μm (mils)
ISO G = 2.5	3.9	(0.15)	6.7	(0.26)	μm (mils)
API 610	1.0	(0.04)	1.8	(0.07)	μm (mils)

Note: 1 μm = 0.001 mm (1 mil = 0.001 in)

The small mass eccentricities, as imposed by API 610, are readily attainable on a state of the art balancing machine. But repeatability of the measured state of balance can hardly be achieved for those low values. If the rotor is put on a different balance machine or balance mandrel, or if the rotor temperature cannot be held totally constant, or if the rotor needs to be reassembled, the tight tolerance will not be maintained without rebalancing. In fact, trim balancing of an assembled rotor where all the components had been balanced individually, may just correct such effects, e.g., a residual shaft bow. The true state of balance may, therefore, become worse with trim balancing.

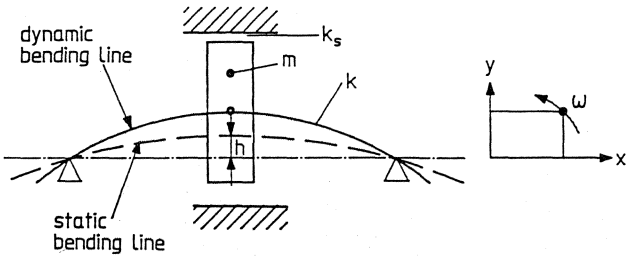

Figure 4. Simple Rotor Model with Bent Rotor, Concentrated Mass and Annular Seal Stiffness.

Bent Shaft

A bent shaft will result in unbalance forces which are in addition to the residual unbalance forces as found on the balancing machine. The bow may have been caused by inappropriate storage of the rotating element (gravitational loads, shocks) or may be temporarily caused by nonsymmetrical thermal expansion, e.g., after a standstill in a hot casing.

The resulting vibrations on the pump will exhibit exactly the same pattern as actual mechanical unbalance and the two phenomena cannot readily be separated. A permanent bow will eventually be detected through dimensional measuring of the rotating element. However, a temporary or thermal bow can only be assumed and is indicated if the operating conditions over time show strong transients or if the element cannot be rotated freely before startup.

To calculate the dynamic forces of a bent shaft, a simplified approach is used [8]:

$$F_b = omega^2 \cdot h_b \cdot k_b \cdot Mass \cdot (Crit\_Speed\_Ratio)^2 \tag{6}$$

where h_b is the maximum shaft bow or eccentricity and k_b is the shape factor which takes into account that not the entire shaft is at the maximum eccentricity. The rotor is assumed to be at about half the maximum eccentricity in one plane as an average along its length, leading to $k_b = 0.5$.

The original bow of the rotor is counteracted by the centering interaction forces at impeller wear rings, balance pistons and/or center piece and throttle bushing. During operation, these elements reduce the initial bow and its induced unbalance forces. It can be shown that the reduction of the bow orbit is about proportional to the square of the ratio of the critical speeds in air and in pumpage, as long as the machine is not run close to the critical speed itself [8]. For a short pump, this ratio is bigger than for a long pump with many wear rings and possibly a center piece in a back to back configuration. In this example, the ratio for the four stage pump is around 0.5 and for the 14 stage pump it is about 0.2.

The simplified calculation allows the following estimate of dynamic forces, induced by a maximum rotor bow of $h_{b,A} = 0.025$ mm (0.001 in) for the four stage pump A and corresponding to Equation (7) $h_{b,B} = 0.057$ mm (0.0023 in) for pump B:

$$h_{b,B} = h_{b,A} \cdot (14+2)/(4+1) \cdot (D_{2,B}/D_{2,A}) \tag{7}$$

taking the number of stages, number of balancing devices, and ratio of impeller diameters into account.

In Table 4, the ratio of forces for pump A and B is much larger than for residual mechanical unbalance, table 2. It becomes quite obvious that the long 14 stage pump B is much less sensitive to a bowed shaft than the short pump A. The lower sensitivity is clearly caused by the influence of the larger number of impeller wear rings and the center piece which straighten the bow of the long rotor to a larger extent than the short rotor.

Table 4. Bent Shaft Excitation Forces.

	Force per Stage		Force of Entire Pump		
	Pump A	Pump B	Pump A	Pump B	
h_b=0.025/57mm	146 (33)	2 (0.5)	585 (131)	30 (7)	N (lb.f.)

Note: TIR = 2 · $h_{b,A}$ = 0.05 mm = 0.002 in
TIR = 2 · $h_{b,B}$ = 0.114 mm = 0.0045 in

Component Runout

On an straight shaft through the geometrical center of the casing, components may have individual runouts. For example, the geometrical center of an impeller or wear ring may not coincide with the center of shaft rotation. In this case interaction forces, i.e., impeller interaction forces [9] and interaction forces at annular seals [10, 11], try to center the component, and therefore, to bend the shaft. This forced whirl causes additional unbalance forces.

In the worst case, the interaction force is strong enough and will center the component totally, introducing an unbalance radius equal to the runout radius. This will tend to be the case for long rotors rather than for short rotors. Then each component can be written:

$$F_{c,\,component} = omega^2 \cdot h_c \cdot k_c \cdot Mass\ (component) \qquad (8)$$

where h_c is the maximum component runout, and k_c is the shape factor which takes into account that not all components are at the maximum eccentricity. As an average, components are assumed to be at about half the maximum eccentricity, though not in one plane, leading to k_b = 0.5.

Unlike on the bowed shaft, it is highly unlikely that all component runouts are in one direction only. It is assumed that all runouts at one impeller are approximately in one direction, and that there are only one or two additional important components, i.e., a balance piston for stacked design or a center piece and a throttle for back to back design. The individual forces now need to be statistically added, which leads to the additional factor $1/\sqrt{(n\_stages + (1 \text{ or } 2))}$ in Equation (9) for the total force. Therefore, in Table 5, "Unbalance Force on Entire Pump" does not correspond to the arithmetic sum of "Unbalance Force per Component,"

$$F_{c,total} = omega^2 \cdot h_c \cdot k_c \cdot Mass / \sqrt{(n\_stages + (1 \text{ or } 2))} \qquad (9)$$

Resulting forces for the two sample pumps can be calculated for the assumption of h_c = 0.013 mm (0.0005 in):

Table 5. Component Run-Out Excitation Forces.

	Force per Component*)		Force of Entire Pump		
	Pump A	Pump B	Pump A	Pump B	
h_c = 0.013 mm	234 (53)	10 (2.3)	523 (118)	41 (9)	N (lb.f.)

*) Number of Components = X Stages + 1 Piston or
= X Stages + 1 Center Piece + 1 Throttle

Note: TIR = 2 · h_c = 0.025 mm = 0.001 in

The forces calculated for pump A are exaggerated, as the interaction forces are unlikely to be strong enough to center the components on the relatively short and stiff rotor. On the long pump B, it can be seen that the influence of component runout becomes stronger than rotor bow.

Hydraulic

Dynamic hydraulic excitation is normally presented in the form of normalized forces and/or pressure pulsations (axial forces are not considered here). While the two are not independent, the normalized forces lend themselves more readily for comparison with mechanical forces. Data on how to measure those forces and results from measurements can be found in [12, 13, 14, and 15]. Generally, the normalized hydraulic excitation force K_H is defined as:

$$K_H = F_H / (rho \cdot g \cdot H \cdot D_2 \cdot B_2^*) \qquad (10)$$

where F_H is the dimensional force, rho is the fluid density, g is the acceleration due to gravity, H is the head, and D_2 and B_2* are the impeller diameter and exit width, respectively.

An overview is given in Figure 5 of measured results for various frequencybands ("fn" is the rotating frequency). Without knowing the individual excitation mechanisms, it can already be seen, that the normalized force K_H depends strongly on the frequency range taken into account and on the flow where the pump is operated.

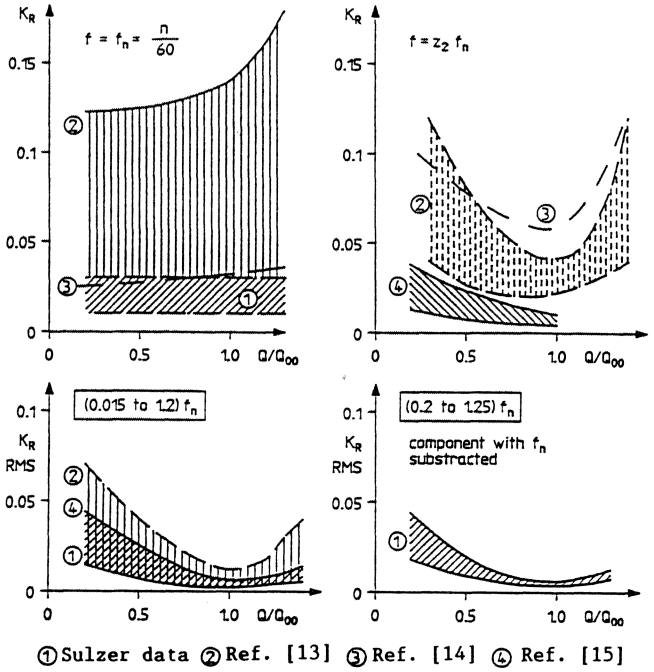

Figure 5. Hydraulic Lateral Excitation Forces.

Note that the narrow frequency band portions of K_H, i.e., at rotating frequency and at vane pass frequency, are given in peak values. Due to the randomness of the broad band portions of K_H, those values are given in RMS values and true peak levels can be up to 3.5 times higher.

Hydraulic Unbalance

There is a portion of the unsteady hydraulic force which is synchronous to the rotating frequency. From Equation (10) it can

be seen that, for a constant synchronous K_H, the dimensional force becomes proportional to the pump head, which in turn is proportional to the square of the rotating speed. Therefore, this hydraulic force behaves exactly the same way as a mechanical unbalance force, and hence, is called hydraulic unbalance.

Measurements of synchronous forces on the pump rotor do not allow the distinction between hydraulic and mechanical unbalance. Similarly to the case of a bent rotor or component runout, other means must be found to differentiate between the various types of unbalance. Hydraulic unbalance can be determined in laboratory tests by running the (short) pump dry and subsequently subtracting the known mechanical unbalance from the one measured during operation (assuming that shaft bow and component runout have been minimized).

For a multistage pump, the only way to identify excessive hydraulic unbalance is by ruling out the mechanical types, and by inspecting the hydraulic passages of the impellers. Hydraulic unbalance forces originate in slight deviations from rotational symmetry of the flow through the impeller channels. This is due to geometrical tolerances, i.e., varying vane exit angles and overall areas between vanes, and some eccentricity of the hydraulic passages relative to the bore of the impeller. The deviations may be small, and not readily detectable during inspection.

Note that hydraulic unbalance cannot be cured by mechanical balancing of the rotor on a mandrel, as the location (phase and amount) of the hydraulic unbalance is not known. Trim balancing in the field lowers the vibration at the measurement location, e.g., at the coupling or at the bearing. As this is not the location where the force originates, the vibrations within the inaccessible wet part of the rotor, at the location of the hydraulic unbalance, may become even worse.

Even for precision cast impellers (ceramic core, lost wax), the normalized hydraulic unbalance is still about $K_{H,u} = 0.015$, see Figure 5, upper left diagram. It can be substantially higher for lower tolerance castings, e.g., sand cast impellers, and according to Verhoeven [13] $K_{H,u}$ can be larger than 0.1.

Gülich, et al. [14], give an example (Figure 6) of measured lateral forces of an impeller with vane exit angles of 36 degrees and for forces of the same impeller with one vane exit angle increased to 51 degrees. It can be seen that the hydraulic unbalance (at f_n) increases up to three fold and more in this extreme example.

The hydraulic unbalance forces for the two sample pumps are calculated and presented in Table 6 for $K_{H,u} = 0.015$. Those forces could easily be two or three times bigger for normal casting impellers.

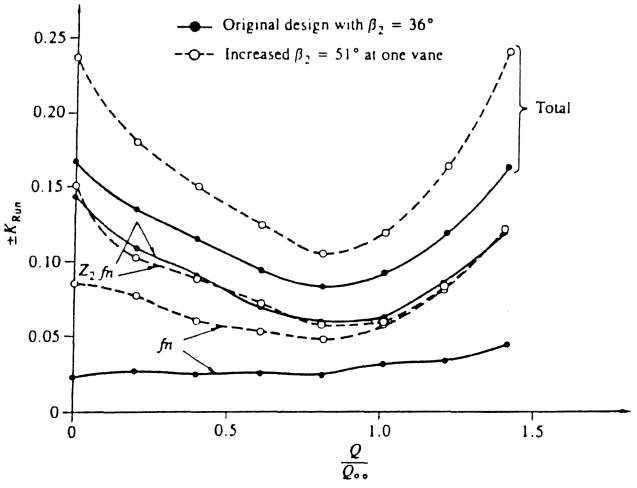

Figure 6. Impeller Tolerances: Unsteady Radial Thrust.

As for the component runout, the resulting force on the entire pump is the statistical sum of the forces per stage, as the forces of individual impellers are not all in the same direction:

$$F_{H,U,stage} = K_{H,U} * (rho \cdot g \cdot H \cdot D_2 \cdot B_2^*) \quad (11)$$

$$F_{H,U,total} = 1/\sqrt{(n\_stages)} \cdot \Sigma\,(F_{H,U,stage}) \quad (12)$$

Table 6. Hydraulic Unbalance Excitation Forces.

	Force per Stage		Force of Entire Pump		
	Pump A	Pump B	Pump A	Pump B	
$K_{H,U} = 0.015$	927 (208)	139 (31)	1854 (417)	519 (117)	N (lb.f.)

The hydraulic unbalance forces for precision cast impellers are substantially bigger on a per stage basis than the mechanical unbalance force for the coarse ISO grade G = 6.3 and of about the same magnitude for the entire pump.

Vane Passage Forces

The cause for vane passing forces can be seen in Figures 7 and 8 [16]. As the vane thickness at the impeller outlet is finite, and there are boundary layers along the vanes, the fluid velocity, and hence the fluid pressure, is not uniform at the impeller outlet. The fluid velocity, w, relative to the impeller has its minimum at the vanes, which in turn makes this the location of the maximum absolute fluid velocity, c. This is due to the rotation of the impeller and the individual directions of the two velocities (see vector diagram in Figure 8). The peaks of the absolute velocity, c, lead to maxima in the stagnation pressure.

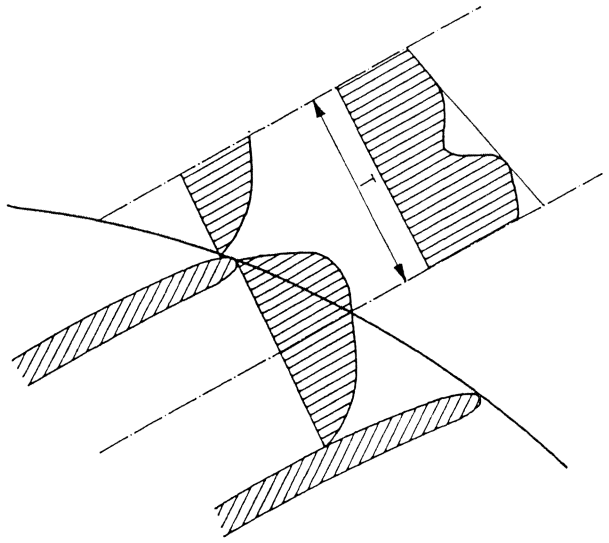

Figure 7. Wake Flow in Impeller Vanes in The Rotating Reference Frame.

With time, as indicated in Figure 7, i.e., further downstream of the impeller outlet, the irregular flow distribution starts to even out. This explains why a larger gap between the impeller outlet diameter and the volute or diffuser inlet diameter leads to lower excitation forces. In Appendix A, Table A2 and Figure A2, an overview is given on the influence of relative clearance between impeller outlet diameter D_2 and volute/diffuser inlet diameter D_3 (Gap "B") on the severity of measured vane pass pressure pulsa-

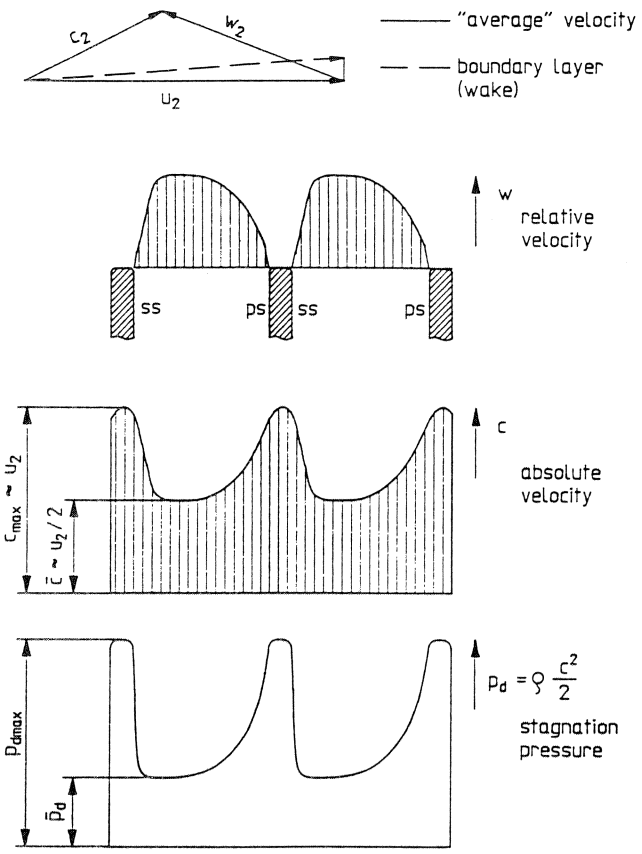

Figure 8. Wake in the Relative and Absolute Coordinate System.

tions, [16]. It has been found that pressure pulsations generally decrease with a power of -0.77 of the relative clearance.

From the flow pattern of Figure 7, it can also be deduced that thinner impeller vanes at the impeller exit lead to narrower disturbances, and therefore, must lead to lower vane pass loading forces. If the vane thickness is decreased to achieve this goal, the minimum thickness to sustain the hydraulic and mechanical vane loads must be taken into account.

These considerations explain why there are uneven pressure distributions at the impeller exit leading to dynamic forces at the frequency of passing vanes. They do not yet explain why some hydraulic designs are more prone to vane pass frequency vibrations than others.

Dubas [17] and Bolleter [18] discuss the phenomenon of vane passing tones in detail. They show the resulting lateral forces for individual combinations of vane numbers in impellers and volutes/diffusers. The derivation is lengthy and for simplicity is not repeated here. However, it can easily be understood that some vane combinations create local pressure pulsations which compensate when integrated around the impeller and some pressure pulsations of other combinations do not compensate. This leads to the most important rule to avoid radial dynamic forces acting on the rotor:

$$n \cdot z_2 - m \cdot z_3 \neq \pm 1, \quad (n, m = 1, 2, 3, \ldots) \qquad (13)$$

where z_2 is the number of impeller vanes and z_3 is the number of volute/diffuser vanes. (N.b., similar rules can be established for axial vibrations and for impeller shroud vibrations). Additionally, to avoid excessive pressure pulsations, the rule given in Equation (14) needs to be respected:

$$n \cdot z_2 - m \cdot z_3 \neq 0, \quad (n, m = 1, 2, 3, \ldots) \qquad (14)$$

In general, combinations with smallest n's and m's are the worst combination. This shows that a three vane impeller in a double volute is very sensitive to vane pass vibrations. The rule of Equations (13) and (14) should be mainly applied with n=m=1 and n, m > 3 are of no practical concern.

It can be seen from Figure 5, upper right diagram, that the normalized vane pass frequency force $K_{R,V}$ (at $f = z_2 \cdot f_n$) depends on the ratio of operating to best efficiency (BEP) flow (Q/Q_{00}). Apparently the unevenness of the flow and pressure distribution at the impeller exit becomes most pronounced and leads to largest forces at very low or very high flows. Though lateral forces at higher harmonics (integer multiples) of vane passing frequency exist (APPENDIX A1), they are not readily quantified.

For the purpose of the two sample pumps, the normalized factor is taken at BEP, $K_{R,V} = 0.025$. Equation (11) applies to calculate vane pass frequency forces at each stage. But Equation (12) cannot be applied to estimate the sum of forces for the entire pump, as impellers normally are staggered per design in a multistage pump. The intention of the stagger is to minimize the sum of the vane pass forces from all stages as far as possible. This is not fully possible, and it is assumed that the compensation of forces by staggering leads to a resulting force inversely proportional to the square root of the number of stages.

$$F_{H,V,total} = F_{H,V,stage} / \sqrt{(n\_stages)} \qquad (15)$$

Table 7. Vane Passing Excitation Forces.

	Force per Stage		Force of Entire Pump		
	Pump A	Pump B	Pump A	Pump B	
$K_{H,V} = 0.025$	1545 (347)	231 (52)	773 (174)	62 (14)	N (lb.f.)

The forces of Table 7 may increase by a factor of 2 to 3, depending on the vane combination of the design, the operating flow, and on the relative impeller - volute/diffuser clearance. The forces on the entire pump will certainly be substantially higher, if the impeller staggering has not been optimized. It also becomes obvious, that vane pass excitation on a single stage pump, where no compensation from one stage to the next is possible, can become predominant for a poor layout.

Forces due to Recirculation/Separation, Rotating Stall, Etc.

Broad band excitation forces are caused by large-scale turbulence, flow separation, and flow recirculation. The typical flow patterns for part load are shown in Figure 9. Most commonly, recirculation or flow separation at the impeller eye is known to occur at low flows, and to increase as the flowrate is reduced towards shutoff. However, recirculation at the impeller outlet volute/diffuser inlet may also be encountered under such conditions. Flow recirculation can lead to various hydraulic effects (cavitation, see below, head increase, etc.), which may be detrimental or beneficial. However, flow recirculation always introduces additional dynamic loading forces on the rotor. This is due to the irregular flow patterns entering the impeller and the volute/diffuser, fluctuations of the flow incidence, fluctuations of the effective through-flow streamline, and large scale pressure fluctuations at the impeller outlet during off BEP flow conditions.

The total lateral forces for varying flows (percent of BEP), [19, 20], on a time base are shown in Figure 10. The randomness and the high levels of the signal at low flows can easily be seen. The

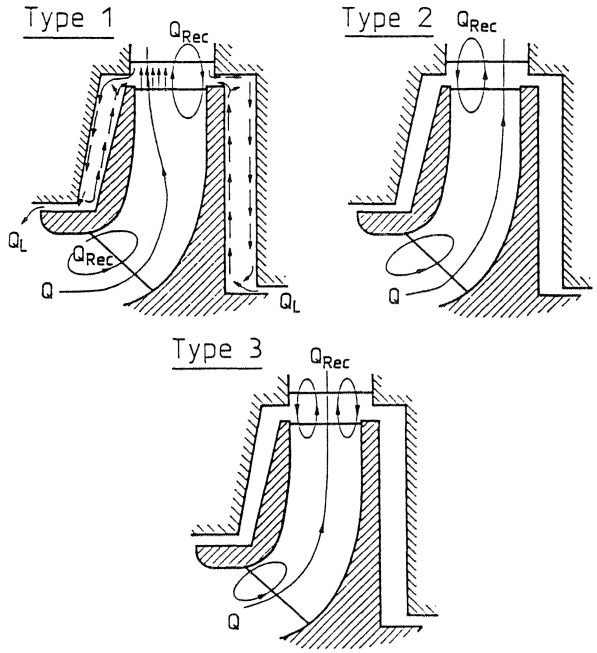

Figure 9. Part Load Flow Patterns.

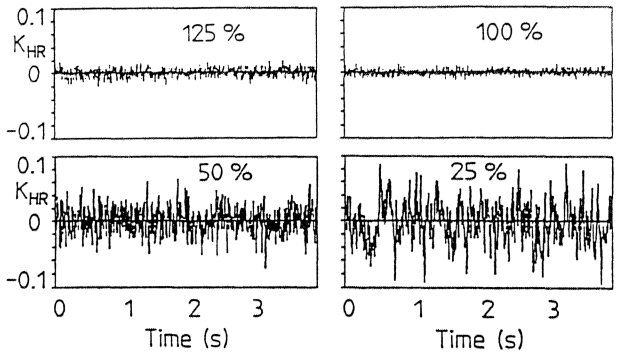

Figure 10. Normalized Radial Broad Band Forces as a Function of Time, for Various Flows.

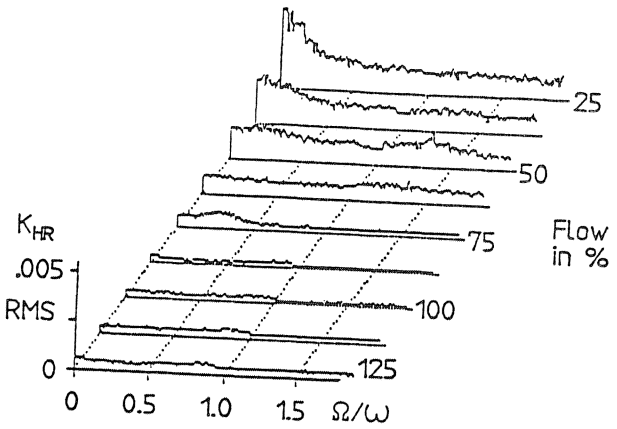

Figure 11. Spectra of Normalized Radial Broad Band Forces, for Various Flows.

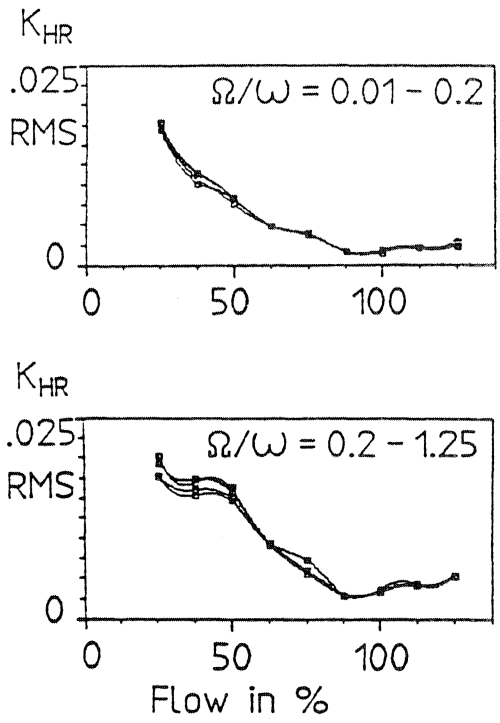

Figure 12. RMS-Values in Two Frequency Bands of Normalized Radial Broad Band Forces.

frequency content of this time base signal is shown in Figure 11. To account for the randomness, RMS-values ("root mean square") are plotted, and the frequency axis is normalized by the rotating frequency. It can be seen that around BEP, the lateral forces are quite small for all frequencies. At low flows, lateral forces increase in general, but they increase strongest at low frequencies. Normally, there is no distinct peak at one given frequency.

In Figure 12, the RMS-values are shown as shown in Figure 11, but integrated into two distinct frequency bands. The results of tests at various speeds and temperatures collapse to one line when normalized, and show that broad band normalized results are repeatable and independent of speed and temperature. The distinct increase of lateral hydraulic forces toward lower flows is also clearly shown in Figure 12.

The example diagrams given here are valid for a certain type of hydraulic design. Other types of hydraulic designs may have other onset points for recirculation with the reduction of flow, and a scatter for the broad band forces will result.

It also has to be noted that there is no rotating stall present in the data of Figures 11 and 12. Though rotating stall occurs at part load, see APPENDIX A1, it is limited to a narrow flow range. Unlike forces due to recirculation, forces due to rotating stall do not keep increasing with the reduction of flow. Furthermore, as the phenomenon is quite repetitive, rotating stall normally produces a lateral force at one fairly steady frequency in the region of 50 percent to 95 percent of running frequency.

Hence, rotating stall is quite an isolated phenomenon which can be identified rather easily (by changing flow; frequency not synchronous, or integer multiple). It is normally the consequence of inappropriate hydraulic design and is not an inherent pump phenomenon. Therefore, while rotating stall has been identified, it is not further treated here.

In the lower part of Figure 5, the RMS-values for the normalized broad band hydraulic excitation forces can be found. The low

frequency band from 1.5 to 20 percent of running frequency and the intermediate frequency band from 20 to 125 percent (excluding 100 percent, which is hydraulic unbalance) indicate both a factor of $K_{H,R} = 0.01$ at BEP. The two forces can be calculated according to Equations (11) and (12) and are indicated in one table only.

Table 8. Broad Band Hydraulic Excitation Forces (RMS-Values).

Low and*) Intermed. Freq. Band	Hydraulic Force per Stage		Hydraulic Force of Entire Pump		
	Pump A	Pump B	Pump A	Pump B	
$K_{H,R} = 0.01$	618 (139)	92 (21)	1236 (278)	346 (78)	N (lb.f.)

*) Note: This is not the sum of the two, but the two are of the same magnitude

Those values, like all hydraulic loading forces, have been calculated at BEP. At small flows, those RMS-forces will be substantially bigger, and peak values may be up to 3.5 times RMS-values, due to the randomness of the forces.

Excitation due to Cavitation

Cavitation is probably one of the most feared and most often discussed detrimental phenomena in centrifugal pumps. [20, 21, 22], and many others cover the various hydraulic aspects of cavitation, its causes, and its effects. Only a general outline for the understanding of the cavitation phenomenon is given here, in order to understand its consequences on pump vibrations.

A typical impeller inlet vane tip and a potential pressure distribution around the inlet are shown in Figure 13. It indicates the available net positive suction head, NPSH, at the suction nozzle which is the margin against vaporization (p_{sat}). As the liquid is accelerated into the impeller inlet, the static pressure is lowered and, if NPSH is insufficient, becomes lower than the vapor pressure in the vicinity of the vane tip. Vapor bubbles formed in this area collapse as soon as they reach an area above vapor pressure further downstream from the inlet. The implosion creates forces which may erode and destroy the vane surface.

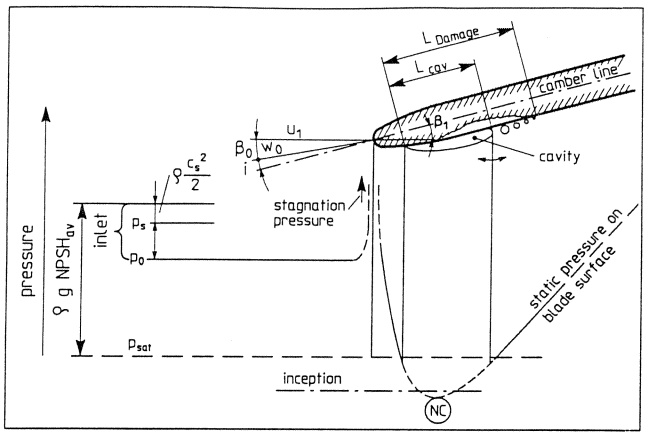

Figure 13. Static Pressure Distribution on a Profile.

There are many other forms of cavitation, beside the one described, [22]: Vortex shedding of an inlet splitter may lead to vapor bubbles being carried from the casing into the impeller eye; recirculation vortices and local vortices in the corners of the impeller channels may lower the static pressure locally below vapor pressure and create vapor bubbles; etc.

As indicated in Figure 14, the formation of cavitation bubbles begins at much higher NPSH (or normalized σ_{u1}) than the generally used NPSH-values for zero percent or three percent head drop would suggest. Therefore, cavitation is present and can be heard even before any head loss can be observed.

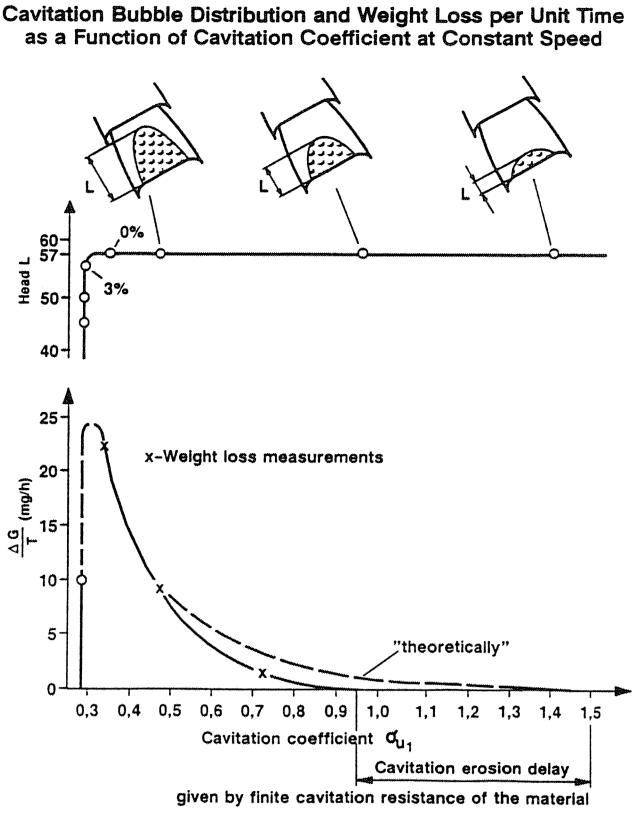

Figure 14. Cavitation Bubbles Vs NPSH.

The clearly audible sound may lead an observer to the conclusion that cavitation is the cause of pump vibrations. But measurement as shown in Figure 15 [14], indicates that overall hydraulic excitation forces, i.e., hydraulic unbalance, vane pass forces, and broad band forces together, do not increase due to cavitation even as three percent head drop is reached. The ratio of hydraulic forces with three percent head drop to the forces without cavitation

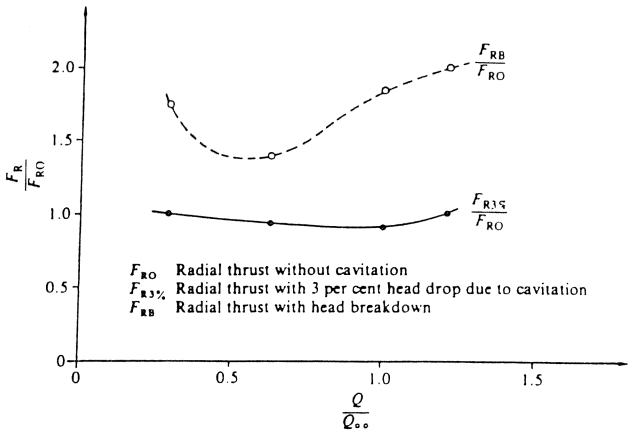

Figure 15. Influence of Cavitation on Lateral Forces.

remains unity over a wide range of flows. Only the hydraulic forces with head breakdown are substantially higher than the forces without cavitation.

There are two reasons for this phenomenon. Firstly, the frequencies for cavitation bubble implosions are very high, generally above 10 kHz. This frequency range is normally not measured (and cannot easily be measured) to determine hydraulic excitation forces or pump vibrations. Secondly, the implosions are highly random events, normally distributed all around the impeller. Additionally, though the stresses induced locally on the vane surface are high enough to destroy the material, the overall forces are not very large.

When the cavitation becomes worse, however, the volume of the vapor bubbles disturbs the normal flow pattern through the impeller to such an extent, that pressure pulsations ("local surges") at frequencies much lower than 10 kHz occur, and eventually the head produced by the impeller breaks down totally. Additionally, large fluctuating vapor cavities will alter the rotational symmetry of lift at impeller vanes and produce lateral forces. Yet, the measured hydraulic forces remain the indirect result of the cavitation, and originate from the pressure pulsations and disturbed flow pattern caused by the large oscillating cavitation bubbles, not their implosion.

A special type of cavitation induced excitation forces occurs mainly with high suction specific speed (large eye/throat area) impellers. Excessive impeller inlet recirculation leads to fluid prerotation upstream of the impeller and hence, to a parabolic pressure profile. The core may be below vapor pressure and block the pipe. The vapor core displaces the fluid and eventually, the flow to the impeller is blocked enough to stop recirculation. Now the prerotation is stopped, the vapor core collapses and the process repeats itself. This unsteady behavior produces lateral loading forces at very low frequencies (<10 Hz) [12].

Strong cavitation normally leads to excessive material erosion and limits the life of the involved parts, mainly the impellers, to short time spans. With big cavitation problems, the focus of attention is normally not on vibrations.

However, cavitation in hydrocarbons does not lead to fast material erosion, and Bolleter, et al.[23], describes a case history of cavitation induced vibration problems and failures on a crude oil pipeline pump. It is noteworthy that shaft vibration readings taken originally, did not indicate any vibration problems. It was only in a later stage that excessive bearing housing vibrations in the range of 20 to 30 times running frequency, i.e., around 1200 to 2000 Hz, were measured (Figure 16). The cause was found to be vortex shedding from the inlet splitter into the impeller eye and blade cavitation leading to strong pressure pulsations. This lead to dynamic forces in the range of above frequencies, a range normally not covered by standard vibration measurement, and to damage of the mechanical seals.

However, actual lateral hydraulic excitation forces directly induced by cavitation are in the range above 10 kHz and are not quantified. Resulting vibrations in this frequency range are so small that they can be neglected. No machine damage is to be expected from forces or vibrations directly induced by cavitation.

Forces indirectly caused by very strong cavitation (close to or at head breakdown) are not easily quantified, but they are also not encountered during normal pump operation.

Surge and System Instabilities

Generally, vibrations caused by surge or system instabilities occur at low frequencies, below 15 Hz and even below 1 Hz. The outlined phenomenon of a vapor core leads to pressure surges at low frequencies.

Other surges can be caused by unfavorable piping-pump system characteristics. Low damped acoustical resonance modes of the liquid in the piping can cause surges [24]. Large system surges can also be caused by waterhammer.

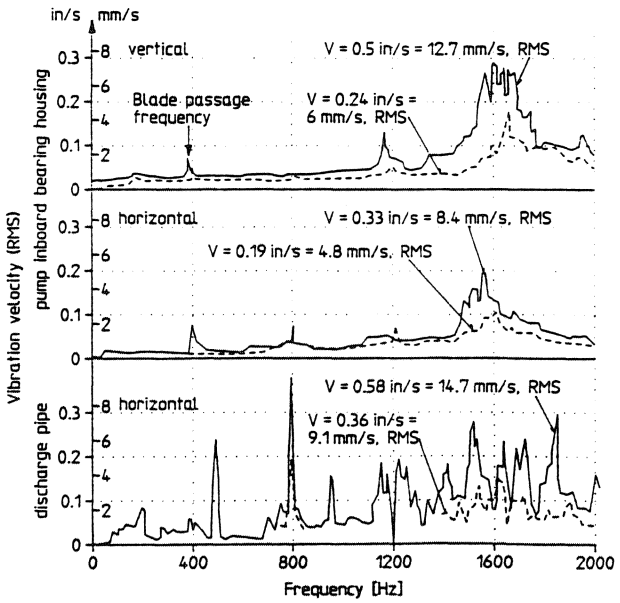

Figure 16. Signature of Indirectly Cavitation Induced Vibrations. (2.48 m³/s at 3320 rpm, solid line; 2.0 m³/s at 3400 rpm, dashed line.)

Transient conditions in hot systems may lead to partial vaporization of the liquid column in the piping system. The subsequent collapse of the vapor volume leads to waterhammer-like forces along the piping.

Head characteristic curves that are flat or rising with increasing flow may lead to system instabilities, depending on the resistance properties of the system. In Figure 17, the possibility of a statically stable (top) and a statically unstable (bottom) combination of a pump and a system characteristic is shown typically. Note that the seemingly unfavorable pump characteristic is the same for both cases, only the combination of the pump and system characteristics defines stable or unstable conditions. Unfavorable head flow characteristics can also cause surges in a system with pumps operating in parallel.

This overview indicates that surges and hydraulic instabilities are mainly system related and not inherent to centrifugal pumps. Surge conditions need to be avoided by appropriate system design and are to be addressed during the design stage. Loading forces caused by surges may vary to a large extent, depending on the type of surge. While some types lead to only slightly elevated vibrations, and maybe annoying noise, others may lead to catastrophic failure (e.g., waterhammer). Hence, while they need to be avoided, surge and system instability caused loading forces cannot be generally quantified, as they do not depend solely on the pump.

COMPARISON OF RESULTS

An overview is given in Table 9 of all the dimensional loading forces estimated for the two sample pumps and Figure 18 shows those results graphically (in N).

General

Comparing the graphs of Figure 18, it becomes quite obvious that all loading forces on the high speed, high energy concentration pump A (top) are substantially larger than on the low energy concentration pump B (bottom). Allowable mechanical unbalance forces increase linearly with the shaft speed and the rotor mass.

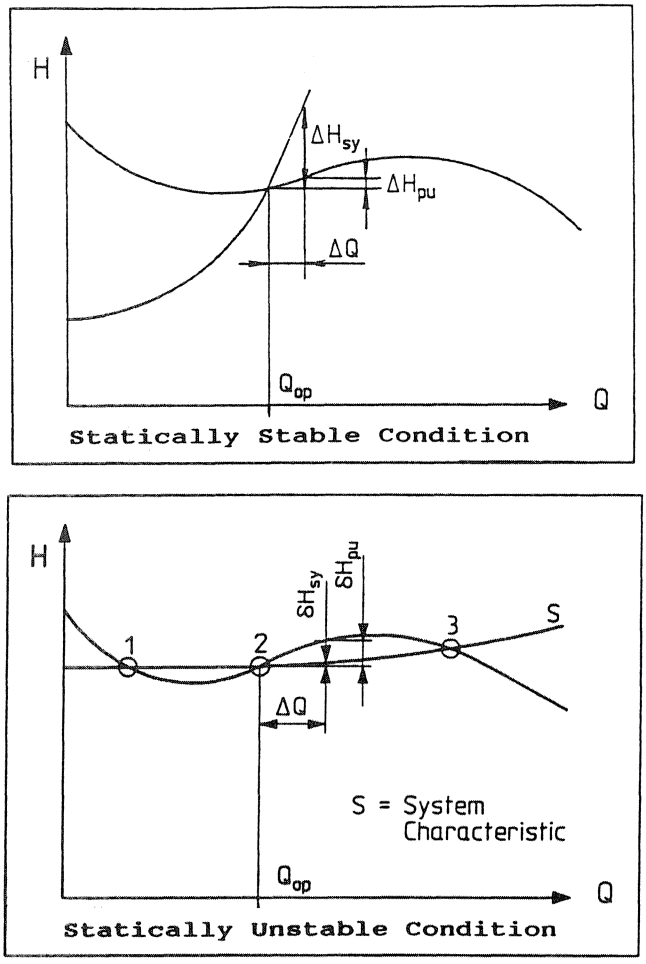

Figure 17. Head-Flow Characteristic against System Characteristic.

Rotor bow, component runout, and hydraulic forces increase with the square of the shaft speed.

This implies that hydraulic forces increase faster with speed than allowable mechanical unbalance forces. However, casting tolerances for low energy impellers are normally much less restrictive than for high energy impellers, leading within the given band width to larger and smaller normalized hydraulic forces. The criteria of allowable tolerances on the impeller cast has not been taken into account for the presented comparison. The difference in

Table 9.

All Forces in N (lb.f.)	Dynamic Loading Force per Stage Pump A	Pump B	Dynamic Loading Force of Entire Pump Pump A	Pump B	Source of Force
ISO G=6.3	454 (102)	32 (7)	1816 (408)	446 (100)	Mechanical
ISO G=2.5	180 (40)	13 (3)	721 (162)	177 (40)	Unbalance
API 610	48 (11)	3 (0.8)	192 (43)	47 (11)	
h_b=0.025/57	146 (33)	2 (0.5)	585 (131)	30 (7)	Bent Shaft
h_c=0.013	234 (53)	10 (2)	523 (118)	41 (9)	Comp. Run-Out
$K_{H,U}$=0.015	927 (208)	139 (31)	1854 (417)	519 (117)	Hyd. Unbalance
$K_{H,V}$=0.025	1545 (347)	231 (52)	773 (174)	62 (14)	Vane Pass
$K_{H,R,l}$=0.01	618 (139)	92 (21)	1236 (278)	346 (78)	Recirc. low f
$K_{H,R,l}$=0.01	618 (139)	92 (21)	1236 (278)	346 (78)	Recirc. int. f

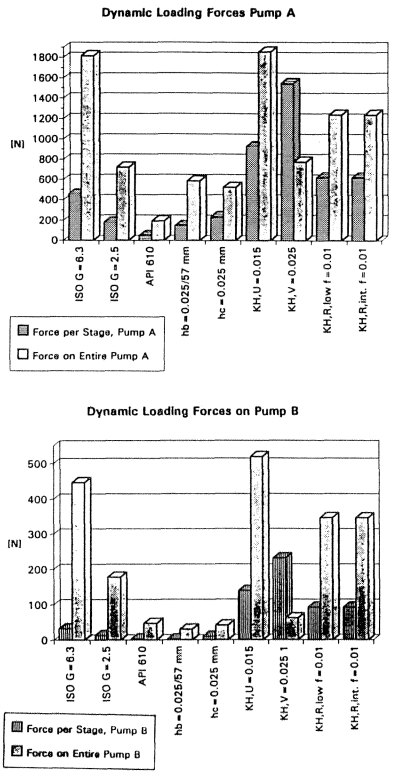

Figure 18. Overview of Sample Loading Forces.

tolerances reduces the stronger speed dependency of hydraulic forces compared to the speed dependency of mechanical forces.

Forces due to a bent shaft or component runout also increase faster with speed than allowable mechanical unbalance forces. But they are generally small and reasonably tight machining tolerances for short rotors are sufficient. Long slender shafts are not as sensitive to a bent shaft or component runout.

The level of dynamic forces acting on the high speed unit A show, that a pump of this type has to be of a sturdy design and that rotordynamic considerations are needed to ensure safe operation. The forces on pump B would suggest that this size and design needs less attention. However, this may be misleading, as the effects counteracting the dynamic loading forces have not been shown for comparison here. Those restoring forces are much larger for pump A than for pump B. Only the calculation of the net balance between excitation and interaction forces can indicate that the operation of pump B is safe, even though the excitation forces appear to be small. However, this requires the discussion of the system characteristics, which is not the scope herein.

Forces Per Stage

For both sample pumps, the hydraulic loading forces on a per stage basis are substantially higher than any of the mechanical loading forces, as clearly shown in Figure 18. Only the mechanical unbalance force for ISO grade G = 6.3 reaches levels that are comparable to hydraulic forces and may have some influence on the vibrational behavior of the rotor. More restrictive residual unbalance limits, i.e., ISO G = 2.5 and API 610, lead to forces per stage which are much smaller than the hydraulic forces, and are of little significance.

The level of the forces resulting from a bent shaft or component runout are about as important as mechanical unbalance forces according to API 610 rules at low speeds and are of the same magnitude as ISO G = 2.5 unbalance forces at high speeds.

On a per stage basis, vane pass frequency forces are strongest, followed by hydraulic unbalance forces and hydraulic broad band forces. This explains why single stage pumps with poor vane combinations and tight lip clearances can exhibit vane pass vibrations which are substantially higher than synchronous unbalance vibrations. The hydraulic broad band forces do not result in a distinct vibration peak and do not affect pump vibrational behavior as strongly as it appears from Figure 18. At lower part load though, the influence of broad band forces is considerably higher, and vibrations induced can become larger than those caused by any other forces.

Forces on Entire Pump

Caused by the different nature of the lateral loading forces and their distribution along the rotor, the total acting force of each category is not necessarily the arithmetic sum of the components acting on each stage. The mechanical unbalance forces and the forces from a bent shaft add arithmetically, the vane pass forces of one impeller are assumed to be partially compensated by additional stages, and the other forces are assumed to add statistically due to their arbitrary direction at each stage.

Hence, some mechanically induced forces become more important as total loading forces on the rotor than on a per stage basis. Yet, even ISO G = 6.3 unbalance forces barely match the hydraulic unbalance forces for both types of pumps. This holds true in spite of the fact that all hydraulic forces were calculated for optimum conditions. Particularly for a pump of the type B, with relatively low head per stage, a cheaper casting for the impellers might be chosen, leading to substantially higher hydraulic unbalance forces than shown here.

With today's generally applied mechanical unbalance limits, i.e., API 610 or similar, the hydraulic unbalance force is clearly the biggest existing dynamic load acting on a pump rotor during normal operating conditions. However, the tight mechanical unbalance limits achieved originally may not easily be maintained.

The effect of tighter balancing limits is shown in Table 10 and Figure 19. The arithmetic sum is the worst case for all unbalance forces being in phase, and the best case with compensating out of phase forces is shown as the arithmetic difference. Both cases are highly unlikely to occur. The statistical sum, the square root of the sum of squares, is the most likely resulting force for arbitrary phases. It can be seen that the tightening of limits from ISO G = 6.3 to G = 2.5 has some impact on the resulting force, but that the tightening from ISO G = 2.5 to API 610 practically does not affect the sum of the forces.

Resulting forces caused by shaft bow and by component runout are of secondary importance on the short pump A, and their influence is negligible on the long rotor of pump B.

The interaction of all synchronous (unbalance) loading forces is quite impressively demonstrated in Figure 19. Tight limits on allowable mechanical unbalance, shaft bow, or component runout hardly reduces the overall synchronous force acting on a stage or on the entire pump. The existing hydraulic synchronous force is predominant and only rather loose mechanical limits affect the resulting force.

Table 10. Resulting Unbalance Forces in [N].

Pump	Mech Unbalance	U_M	Bent Shaft	Comp. Run-Out	Hydr. Unb.	Arith. Sum	Arith. Diff.	Stat. Sum
A	ISO G=6.3	1816	585	523	1854	4778	24	2711
	ISO G=2.5	721	585	523	1854	3683	25	2138
	API 610	192	585	523	1854	3154	554	2022
B	ISO G=6.3	446	30	41	519	1036	2	686
	ISO G=2.5	177	30	41	519	767	271	550
	API 610	47	30	41	519	637	401	524

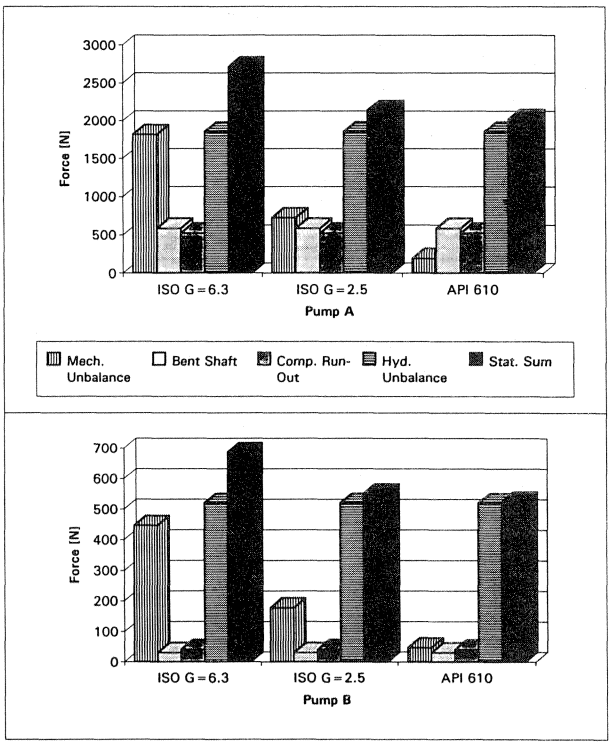

Figure 19. Resulting Unbalance Forces for Various Mechanical Balance Grades.

As expected from the intentional impeller stagger, the vane pass frequency forces become smaller as an overall force on the rotor. The effect of vane pass forces on a 14 stage pump is small, if adequate design rules have been used.

Broad band excitation forces are important at off BEP flow conditions. At very low flows, broad band vibrations can become predominant, and can be higher than any other vibrations.

CONCLUSIONS

The most important dynamic loading forces acting on a pump rotor have been shown and their nature explained. Estimates for inherent forces have been given at the example of two typical pump designs. It has been shown that hydraulic excitation forces in a pump generally are predominant.

The influence of rotor bow or component runout is considerably smaller on a long, slender shaft than on short, stiff shaft. However, if bow and runout are maintained within reasonable limits, those forces are of secondary importance.

The lowest level of hydraulic forces has been calculated, based on measured results on impellers with tight casting tolerances (ceramic core, lost wax). In comparison, mechanical unbalance induced vibrations with limits as imposed by API are much smaller. In light of this comparison, the stringent API limits, for which repeatability can hardly be maintained, do not appear to be necessary. Even the less stringent ISO grade G = 2.5 results in forces on the rotor which are considerably lower than the predominant hydraulic unbalance forces. Balancing a rotor to less than G = 2.5 will therefore not further reduce synchronous vibrations. In many cases, i.e., with more economic lower precision casting impellers for lower heads per stage, a balancing level of G = 6.3 may be sufficient.

Vane pass frequency forces have been shown to be high for a single stage, but on a multistage pump forces compensate to a certain extent by appropriate staggering of the impellers. A general

rule about favorable impeller volute/diffuser vane combination has been indicated, and with the help of measured results, the importance of a sufficient impeller volute/diffuser clearance ("Gap B") has been shown.

The nature of hydraulic broad band excitation forces has been explained to be caused mainly by flow recirculation. These forces are distributed over a wide frequency band, and do not cause a distinct vibration peak, but contribute to overall vibration. At low pump flows, measured results show that broad band vibrations can reach levels higher than unbalance induced vibrations.

Mechanisms leading to surge and system instability have been outlined. Typical levels for loading forces cannot be indicated for this type of excitation as they depend strongly on the system design. However, it has been realized that those low frequency pulsations may be of catastrophic levels, and need to be addressed during the design stage of the system.

RECOMMENDATIONS

Based on the discussion of the dynamic loading forces presented, a summary and recommendations can be established, see Tables 11 and 12. These are general guidelines and more detailed information on individual forces and mechanisms can be found in literature.

Typical values are shown in Table 11 to estimate loading forces acting on a centrifugal pump. The recommended value is a statistical average which may change considerably with individual designs and manufacturing tolerances. This is indicated by the relative broad range of possible minimum and maximum values. The recommendation for residual unbalance limits are given assuming that all other forces are in their lower range. Further limiting the unbalance will not reduce the resulting overall loading forces on the pump.

Some potential solutions to reduce individual loading forces are summarized in Table 12. Only vibrations caused by loading forces are considered, and system related problems are not included (compare to APPENDIX A1).

Table 11.

Source of Force	Grades / Condition	Recommended Values	Poss. Values *) Min.	Max.
Mechanical Unbalance	Component Rotor	G = 2.5 G = 2.5 - 6.3		
Bent Shaft (bare shaft)	± 5 stages TIR = ± 10 stages µm (mils)	25 - 50 (1 - 2) 50 - 75 (2 - 3)		
Comp. Run-Out (OD to bore)	(All) TIR µm (mils) = (incr. w/ lower speed)	25 - 65 (1 - 2.5)		
Hyd. Unbalance (radial thr.)	All Q, Prec. Cast Imp. All Q, Norm. Cast Imp.	0.015 0.03	0.01 0.02	0.025 0.05
Vane Pass (radial thrust)	Q/Q_{BEP} = 0.25 Q/Q_{BEP} = 0.50 Q/Q_{BEP} = 1.0 Q/Q_{BEP} = 1.25	0.035 0.03 0.025 0.03	0.025 0.015 0.01 0.02	0.08 0.06 0.04 0.06
Recircircul. low frequency (radial thrust)	Q/Q_{BEP} = 0.25 Q/Q_{BEP} = 0.50 Q/Q_{BEP} = 1.0 Q/Q_{BEP} = 1.25	0.04 0.025 0.01 0.015	0.015 0.01 0.005 0.005	0.06 0.04 0.015 0.025
Recircircul. intermed. fr. (radial thrust)	Q/Q_{BEP} = 0.25 Q/Q_{BEP} = 0.50 Q/Q_{BEP} = 1.0 Q/Q_{BEP} = 1.25	0.035 0.02 0.01 0.015	0.02 0.01 0.005 0.005	0.04 0.025 0.015 0.02

*) Those are not the absolute Minimum and Maximum values attainable, but extreme values estimated possible with normal manufacturing quality.

Table 12.

Source of Force	Identification	Recommendations to lower Vibrations
Mechanical Unbalance	Peak at rotational frequency f_N = N/60. (Check if not hyd. unb., shaft bow, excessive run-out) Increases with speed. Not flow dependent.	- Only couplings may be trim balanced (coupling dominated critical speed?) Rotor trim balance may lead to higher vibrations in wet part - Balance individual components on rotor
Bent Shaft	Peak at rotational frequency f_N = N/60. (see mech. unb.)	- Check shaft run-out and correct - Check for thermal transients (temporary thermal bow)
Comp. Run-Out	Peak at rotational frequency f_N = N/60. (see mech. unb.)	- Check component run-out, loose fits, non-symmetric parts (thermal growth)
Hyd. Unbalance	Peak at rotational frequency f_N = N/60. (see mech. umb.)	- Check impeller dimensions (throat areas, vane angles) - Higher precision imp. casting.
Vane Pass	Peak at vane passage frequency and multiples ($z_2 \cdot f_N$, $2 \cdot z_2 \cdot f_N$, $3 \cdot z_2 \cdot f_N$,...) Flow dependent.	- Check the rule for vane combin. $n \cdot z_2 - m \cdot z_3 \neq \pm 1$ (n, m = 1, 2,...) $n \cdot z_2 - m \cdot z_3 \neq 0$ (n, m = 1, 2, 3,...) - Check the relative lip clearance Gap B = $D_3/D_2 - 1 > 4\%$ (6 diff.) - Thinner impeller exit vanes - Profiled volute/diffuser vanes - Check against low flow
Recirc. low f Recirc. int. f	no distinct peak, broad band vibrations 0 to 1.5 · f_N, increas. towards lower freq. Strongly flow depend.	- Check against low flow - Check against high suc. spec. speed n_{ss}, large impeller eye - Increase min. flow - Install "Anti-Stall" ring
Rotating Stall	Peak around 0.5 to 0.95 · f_N. Freq. prop. to speed. Amplitude increases slightly with speed. Flow dep.	- Change flow - Improve hydraulic design.
Cavitation (indirectly)	Broad band vibrations around 0.5 to 10 kHz Strongly suction pressure dependent.	- Reduce cavitation induced pres. pulsation by increasing suct. pressure (NPSH) - Improve hydraulic design.
Surge and System Instability	Relatively distinct peak at low frequency below 15 Hz to less than 1 Hz	- Check on acoustic resonance of system pipe - pump. - Check on parallel running pumps (head - flow characteristics) - Check for flat or rising head - flow characteristic.

Vibrations induced by loading forces may be amplified due to system resonances. In this case, vibrations may remain high, even if the loading forces are minimized (they cannot be eliminated totally). For example, repeated rotor balancing will not reduce synchronous vibrations significantly if the pump is running at or close to a critical speed; cutting impeller vanes back may not resolve high vane pass frequency vibrations on a bearing housing, if the housing is resonant around this frequency; etc. Hence, the following recommendations are to be used if no resonant conditions exist. For resonant conditions, either the system resonance frequency or the excitation frequency needs to be changed, before any other changes are attempted.

APPENDIX A

Table A1. Classification of Root Causes of Vibration Problems in Multistage Pumps

Case N° (Fig.A1)	Observed Phenomenon	Root cause: System-related	Root cause: Excitation related
1	Peak at rotational frequency f_n (synchronous vibrations)	-Critical speed, low damping -Bearing housing or pump casing structural resonance (excited by residual unbalance)	-Mech. unbalance -Hydraulic unbalance -Bent rotor -Excessive run-out of components
2	Peak(s) at low multiple or fraction of rotational frequency ($2 \cdot f_n$, $f_n/2$ etc.)	-Nonlinearities due to: loose parts, loose bearings, rubbing etc.	-Misalignment (sometimes causing f_n only)
3	Peaks(s) at blade passage frequency and multiples ($z_2 \cdot f_n$, $2z_2 \cdot f_n$...)	-Internal acoustic resonance (excited by blade interaction)	-Interaction unfavorable blade numbers, insufficient radial gap, extreme off-design flow
4	Relatively distinct peak at a frequency $0.5 \cdot f_n$...$0.95 \cdot f_n$ (subsynchronous vibration)	-Rotor instability, incl. "bearing" instability, i.e. damping of particular mode is around zero or negative. Often occurs at worn clearances. Occurs at all flows frequency increasing with speed. Amplitude "jumps" to destructive levels above certain speed.	-Periodic hydraulic excitation forces, rotating stall and similar phenomena, occur at part load in a relatively narrow flow range, frequency proportional to speed Amplitude slightly increasing with speed
5	Broad band vibrations at less than about $0.2 \cdot f_n$, usually increasing towards lower frequencies	-	-Broad band hydraulic forces due to unsteady flows (recirculation, turbulence) usually at part load
6	Relatively distinct peak at low frequency usually below 15 Hz, down to less than 1 Hz	-Low or negatively damped acoustical modes of the liquid in the pipe system due to flat or rising head-flow curve -Surges in the hydraulic system due to parallel operation of pumps with unfavorable head flow curves -Instability in feedwater control system	-Excitation of hydraulic nature: -Axial shuttling due to position-dependent axial thrust forces -Broad band hydraulic forces exciting low frequency structural resonances (elastic foundations, pipes)
7	Broad band vibrations between 0.5 KHz and 10 KHz - and higher, strongly dependent on suction pressure	-	-Cavitation induced pressure pulsations and vibrations
8	Peak at 1x or 2x line frequency or other exact multiples of line frequency		-Motor vibrations transmitted to the pump via foundation or shaft
9	Relatively broad peak at a frequency not related to rotational frequency		-Casing or bearing housing resonance excited by broad band turbulent forces

Figure A1. Illustrative Vibration Spectrum of a Pump at 3560 RPM, Indicating Various Vibration Phenomena. Impellers have 5 Blades, Line Frequency is 60 Hz. Explanations see Table A1.

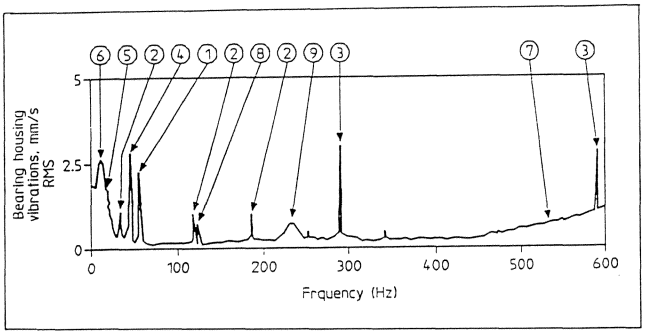

Table A2. Influence of Radial Gap Between Impeller and Diffuser/ Volute on Pressure Pulsations and Stresses.

	Measured Quantity	Location	Comment		|m|
1	Instationary Stagnation Pressure	Diffuser Leading Edge	Local		0.62
2			Average		0.63
3		Annular Discharge Casing	Low Flow		0.81
4			High Flow		0.92
5	Pressure Pulsations	Diffuser Inlet	$\frac{Q}{Q_{BEP}}$	0.6	0.65
6				1.0	0.95
7		Volute		0.5	
8				1.0	
9	Instationary Stress in Diffuser Vane	Diffuser Leading Edge	1/10 of Measured Stresses are Plotted		0.78

Peak-to-peak values at blade passing frequency normalized according to:

$$dp^* = \left[\frac{dp}{\frac{u_2^2}{rho \cdot \frac{2}{}}} \right] \qquad \text{Gradient m: } dp^* = \left[\frac{D_3}{D_2} - 1 \right]^{-m}$$

Figure A2. Influence of Radial Gap Between Impeller and Diffuser/Volute on Pressure Pulsations and Stresses (see Table A2 for Explanations).

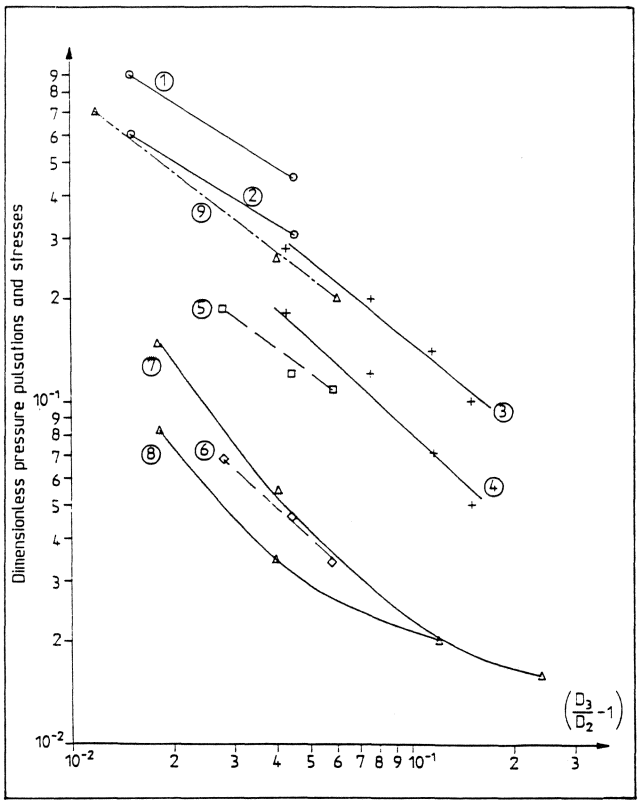

REFERENCES

1. Bolleter, U. and Frei., A., "How to Ensure Good Rotordynamic Behavior of High Energy Multistage Pumps," EPRI Power Plant Pumps Symposium, Tampa Florida (June 1991).
2. Bolleter, U. and Florjancic, D., "Predicting and Improving the Dynamic Behavior of Multistage High Performance Pumps," *Proceedings of the First International Pump Symposium*, Turbomachinery Laboratory, Department of Mechanical Engineering, Texas A&M University, College Station, Texas (1984).
3. Pace, S.E., Florjancic, S., and Bolleter, U., "Rotordynamic Developments for High Speed Multistage Pumps," *Proceedings of the Third International Pump Symposium*, Turbomachinery Laboratory, Department of Mechanical Engineering, Texas A&M University, College Station, Texas (1986).
4. Bolleter, U., Frei, A., Florjancic, S., Leibundgut, E., and Stürchler, R., "Rotordynamic Modelling and Testing of Boiler Feed Pumps," EPRI Research Project 1884-10, Final Report (April 1991).

5. Marscher, W.D., "How to Use Impact Testing to Solve Pump Vibration Problems," EPRI Power Plant Pumps Symposium, Tampa Florida (June 1991).
6. International Standard ISO 1940, Balance Quality of Rotating Rigid Bodies, First Edition (1973).
7. API Standard 610, Seventh Edition, Centrifugal Pumps for General Refinery Service (February 1989).
8. Bolleter, U. and Frei, A., "Causes and Control of Synchronous Vibrations of Multistage Pumps," IMechE, London GB (December 1990).
9. Bolleter, U., Leibundgut, E., and Stürchler, R., "Hydraulic Interaction and Excitation Forces of High Head Pump Impellers," Proceedings of the 3rd Joint ASCE/ASME Mechanics Conference: Pumping Machinery Symposium, San Diego (July 1989).
10. Childs, D.W., "Finite Length Solution for Rotordynamic Coefficients of Turbulent Annular Seals," ASME Transaction Journal of Lubrication Technology, pp. 437-444, *105* (July 1983).
11. Florjancic, S., "Annular Seals of High Energy Centrifugal Pumps: A New Theory and Full Scale Measurement of Rotordynamic Coefficients and Hydraulic Friction Factors," Ph.D. Thesis, Federal Institute of Technology (ETH) Zürich, Switzerland, Number 9087 (May 1990).
12. Gülich, J.F., "Part Load Flow Phenomena and Excitation Forces in Centrifugal Pumps," Conference on Vibration and Wear in High-Speed Turbomachinery, Lisbon, Portugal (April 1989).
13. Verhoeven, J., "Unsteady Hydraulic Forces in Centrifugal Pumps," Conference on Partload Pumping, Edinburgh, Scotland, Instn. Mech. Engr. Paper C348/88 (1988).
14. Gülich, J.F., Jud, W., and Hughes, S.F., "Review of Parameters Influencing Hydraulic Forces on Centrifugal Impellers," Proc. Instn. Mech. Engrs., *201* (A3), pp. 163-174 (1987).
15. Kanki, H., et al., "Experimental Research on the Hydraulic Excitation Force on the Pump Shaft," ASME Paper 81-DET-71 (1981).
16. Gülich, J.F. and Bolleter, U., "Pressure Pulsations in Centrifugal Pumps," ASME Journal of Vibrations and Acoustics, *114*, pp. 272-279 (April 1992).
17. Dubas, M., "Über die Erregung infolge Periodizität von Turbomaschinen," Ingenieur-Archiv *54*, pp. 413-426, Springer Verlag (1984).
18. Bolleter, U., "Blade Passage Tones of Centrifugal Pumps," Vibrations, *4* (3), pp. 8-13 (1988).
19. Bolleter, U., Leibundgut, E., Stürchler, R., and McCloskey, T., "Hydraulic Interaction and Excitation Forces of High Head Pump Impellers," Third Joint ASCE/ASME Mechanics Conference, University of California, San Diego, California (July 1989).
20. Gülich, J.F., Bolleter, U., and Simon, A., "Feedpump Hydraulic Performance and Design Improvement-Project Summary Report," EPRI RP 1884-10, Final Report (February 1992).
21. Gülich, J.F., "Guidelines for Prevention of Cavitation in Centrifugal Feedpumps," EPRI GS-6398 (1989).
22. Schiavello, B. and Prescott, M., "Field Cases Due to Various Cavitation Damage Mechanisms: Analysis and Solutions," EPRI Power Plant Pumps Symposium, Tampa, Florida (June 1991).
23. Bolleter, U., Schwarz, D., Carney, B., and Gordon, E.A., "Solution to Cavitation Induced Vibration Problems in Crude Oil Pipeline Pumps," *Proceedings of the Eighth International Pump Users Symposium*, Turbomachinery Laboratory, Department of Mechanical Engineering, Texas A&M University, College Station, Texas (1991).
24. Bolleter, U., Stirnemann, A., Eberl, J., and McCloskey, T., "The Dynamic Transfer Matrix of a Pump and Its Use in Pumping System Design," ISROMAC-3, Honolulu, Hawaii (1990).